Numerical Simulation of Transient Heat Conduction in a Rocket Nozzle Wall

Riyad Babayev*, Gregor P. McKenzie†, Hamza Rimawi‡, and Bradley Wassef§
University of Illinois Urbana-Champaign, Urbana, IL, 61801

This project models and simulates one-dimensional transient heat conduction in a solid slab. It is done using finite-element-style spatial discretization and the trapezoidal rule for time integration. The system is subject to fixed boundary temperatures that represent extreme thermal conditions. A mass matrix and stiffness matrix formulation is used to construct the semidiscrete system. The numerical method is verified through a convergence study, confirming the second-order spatial accuracy. The results highlight the stability and effectiveness of the implicit scheme in capturing the heat diffusion behavior over time.

Nomenclature

$u(x,t)$	=	Temperature as a function of space and time [K]
T_0	=	Initial temperature of the slab [K]
T_{gas}	=	Boundary temperature at the hot gas side [K]
T_{coolant}	=	Boundary temperature at the coolant side [K]
L	=	Length of the slab [m]
α	=	Thermal diffusivity [m^2/s]
k	=	Thermal conductivity [$\text{W}/\text{m} \cdot \text{K}$]
ρ	=	Density [kg/m^3]
c_p	=	Specific heat at constant pressure [$\text{J}/\text{kg} \cdot \text{K}$]
Δx	=	Spatial grid spacing [m]
Δt	=	Time step [s]
t_{end}	=	Final simulation time [s]
n	=	Number of interior spatial nodes
M	=	Mass matrix in FEM discretization
A	=	Stiffness matrix in FEM discretization
$\mathbf{g}(t)$	=	Boundary condition forcing vector
$\mathbf{u}$	=	Temperature vector at interior nodes
I	=	Identity matrix
RHS	=	Right-hand side of trapezoid method system
LHS	=	Left-hand side matrix of trapezoid method system
u^k	=	Temperature vector at time step k
t	=	Time [s]
x	=	Spatial coordinate [m]
$\|\| \cdot \|\|_2$	=	Discrete L_2 norm of error

I. Introduction

Understanding how heat diffuses through materials is essential in many engineering applications, from aerospace thermal protection systems to electronic device cooling. In particular, one-dimensional transient heat conduction provides a simplified yet powerful framework to model thermal behavior in thin solids or layered components. Although

*Undergraduate Student, Department of Aerospace Engineering
†Undergraduate Student, Departments of Aerospace Engineering and Astronomy
‡Undergraduate Student, Department of Aerospace Engineering
§Undergraduate Student, Department of Aerospace Engineering

analytical solutions exist for specific cases, most realistic engineering problems require numerical techniques to handle complex boundary conditions, material properties, or geometries.

In this project, we investigate the unsteady heat conduction in a thin slab where one end is exposed to a high temperature gas stream and the other to a coolant. The goal is to simulate how temperature evolves over time within the slab under these boundary conditions. To solve this initial boundary value problem (IBVP), we use a finite element-style method for spatial discretization, forming a mass and stiffness matrix. For time integration, we apply the trapezoidal rule, an implicit second-order accurate method known for its stability and robustness in solving stiff systems.

The project includes verification through a convergence study, in which the numerical error is measured across multiple grid sizes and compared against a refined reference solution. The performance and accuracy of the method are evaluated with respect to both spatial and temporal discretization parameters.

II. Problem Description

This project models transient one-dimensional heat conduction through a thin slab subjected to extreme temperature gradients at its boundaries. Such a configuration is representative of high-temperature environments in engineering systems, such as thermal barrier coatings in aerospace components or heat exchangers in energy systems. Understanding how heat propagates in these materials is essential to prevent structural damage, maintain efficiency, and ensure safety.

The slab is assumed to be homogeneous and of length $L = 0.01$ m, with thermal diffusivity $\alpha = 10^{-5}$ m^2/s. The left boundary is held at a high temperature ($T_{\text{gas}} = 2000$ K) to simulate exposure to combustion gases, while the right boundary is maintained at a lower coolant temperature ($T_{\text{coolant}} = 300$ K). The initial temperature of the slab is uniform at $T_0 = 300$ K.

The governing partial differential equation (PDE) is the one-dimensional heat equation:

$$\frac{\partial u}{\partial t} = \alpha \frac{\partial^2 u}{\partial x^2}, \quad x \in (0, L), \quad t > 0 \tag{1}$$

with the following conditions:

$$u(x, 0) = T_0 \quad \text{(initial condition)} \tag{2}$$

$$u(0, t) = T_{\text{gas}}, \quad u(L, t) = T_{\text{coolant}} \quad \text{(Dirichlet boundary conditions)} \tag{3}$$

The primary parameter ranges explored include spatial discretizations with $n = 10$ to 160 interior points and a fixed time step of $\Delta t = 10^{-4}$ s over a final simulation time of $t_{\text{end}} = 1.0$ s.

III. Numerical Method

We solve the one-dimensional heat equation

$$\frac{\partial u}{\partial t} = \alpha \frac{\partial^2 u}{\partial x^2} \tag{4}$$

on the domain $x \in [0, L]$, with Dirichlet boundary conditions. The problem is discretized in space using a finite element-style approach with piecewise linear basis functions, resulting in a semi-discrete system of ordinary differential equations (ODEs). The resulting formulation is:

$$M \frac{d\mathbf{u}}{dt} = A\mathbf{u} + \mathbf{g}(t) \tag{5}$$

where:

- $\mathbf{u}(t) \in \mathbb{R}^n$ is the temperature vector at the interior nodes,
- $M \in \mathbb{R}^{n \times n}$ is the mass matrix,
- $A \in \mathbb{R}^{n \times n}$ is the stiffness matrix,
- $\mathbf{g}(t)$ accounts for Dirichlet boundary condition contributions.

A. Spatial Discretization: Mass and Stiffness Matrices

Let $\Delta x = L/(n+1)$ be the uniform spacing between the n interior nodes. The mass and stiffness matrices are defined as:

Mass matrix:

$$M = \frac{\Delta x}{6}\begin{bmatrix} 4 & 1 & 0 & \cdots & 0 \\ 1 & 4 & 1 & \ddots & \vdots \\ 0 & 1 & 4 & \ddots & 0 \\ \vdots & \ddots & \ddots & \ddots & 1 \\ 0 & \cdots & 0 & 1 & 4 \end{bmatrix} \tag{6}$$

Stiffness matrix:

$$A = \frac{\alpha}{\Delta x}\begin{bmatrix} -2 & 1 & 0 & \cdots & 0 \\ 1 & -2 & 1 & \ddots & \vdots \\ 0 & 1 & -2 & \ddots & 0 \\ \vdots & \ddots & \ddots & \ddots & 1 \\ 0 & \cdots & 0 & 1 & -2 \end{bmatrix} \tag{7}$$

Boundary vector:

$$\mathbf{g}(t) = \frac{\alpha}{\Delta x}\begin{bmatrix} T_{\text{left}}(t) \\ 0 \\ \vdots \\ 0 \\ T_{\text{right}}(t) \end{bmatrix} \tag{8}$$

B. Time Discretization with the Trapezoidal Rule

To integrate the semi-discrete system in time, we apply the trapezoidal rule (a second-order accurate, implicit method). The time-stepping formula is:

$$M\frac{\mathbf{u}^{k+1} - \mathbf{u}^k}{\Delta t} = \frac{1}{2}\left[A\mathbf{u}^k + A\mathbf{u}^{k+1} + \mathbf{g}^k + \mathbf{g}^{k+1}\right] \tag{9}$$

Multiplying through by Δt and rearranging:

$$M\mathbf{u}^{k+1} - \frac{\Delta t}{2}A\mathbf{u}^{k+1} = M\mathbf{u}^k + \frac{\Delta t}{2}A\mathbf{u}^k + \frac{\Delta t}{2}\left(\mathbf{g}^k + \mathbf{g}^{k+1}\right) \tag{10}$$

Defining the left-hand side and right-hand side:

$$LHS = M - \frac{\Delta t}{2}A \tag{11}$$

$$RHS = M\mathbf{u}^k + \frac{\Delta t}{2}A\mathbf{u}^k + \frac{\Delta t}{2}\left(\mathbf{g}^k + \mathbf{g}^{k+1}\right) \tag{12}$$

Then, the update rule is:

$$LHS \cdot \mathbf{u}^{k+1} = RHS \tag{13}$$

C. Method Justification and Properties

The trapezoidal rule is unconditionally stable for linear problems (A-stable) and second-order accurate in time. Combined with the finite element spatial discretization, this yields a method that is accurate and robust for solving parabolic PDEs such as the heat equation. Additionally, the system matrix LHS remains constant throughout the simulation, allowing its factorization to be reused at every time step, reducing computational cost.

D. Algorithm Summary

Given n interior nodes, time step Δt, and final time t_{end}:

1) Construct matrices M and A.
2) Initialize $\mathbf{u}^0 = T_0 \cdot \mathbf{1}$.
3) Precompute $LHS = M - \frac{\Delta t}{2} A$ and factor it.
4) For each time step $k = 0, 1, \ldots, N-1$:
    1) Compute $\mathbf{g}^k$ and $\mathbf{g}^{k+1}$ from boundary conditions.
    2) Assemble $RHS = M\mathbf{u}^k + \frac{\Delta t}{2} A\mathbf{u}^k + \frac{\Delta t}{2}(\mathbf{g}^k + \mathbf{g}^{k+1})$.
    3) Solve $LHS \cdot \mathbf{u}^{k+1} = RHS$.

IV. Implementation and Verification

The numerical method was implemented in Python using a custom solver that combines finite-element-style spatial discretization with the trapezoidal rule for time integration. The slab was discretized into n interior nodes with uniform spacing, and temperature values were tracked at each node over time.

The system of equations takes the form:

$$M\frac{d\mathbf{u}}{dt} = A\mathbf{u} + \mathbf{g}(t) \tag{14}$$

where $\mathbf{u}(t)$ is the temperature vector, M is the mass matrix, A is the stiffness matrix, and $\mathbf{g}(t)$ is the boundary forcing vector. The matrices M and A are tridiagonal and constructed using standard formulas for linear basis functions. The boundary vector updates at each time step based on the applied temperature conditions.

To advance the solution in time, we use the trapezoidal rule:

$$\mathbf{u}^{k+1} = \left(I - \frac{\Delta t}{2} M^{-1} A\right)^{-1} \left[\mathbf{u}^k + \frac{\Delta t}{2} M^{-1} \left(A\mathbf{u}^k + \mathbf{g}(t^k) + \mathbf{g}(t^{k+1})\right)\right] \tag{15}$$

The matrix on the left-hand side remains constant during simulation and is pre-inverted for efficiency. At each time step, the right-hand side is assembled and the system is solved to update $\mathbf{u}^{k+1}$.

We verified the method using a convergence study. A reference solution was generated using a fine grid ($n = 160$) and small time step ($\Delta t = 5 \times 10^{-4}$ s). Coarser simulations were compared to this reference to evaluate accuracy.

For spatial convergence, $\Delta t = 10^{-4}$ s was fixed and n was varied from 10 to 80. The L_2 error at final time was measured and plotted versus Δx on a log-log scale. The observed convergence rate matched the expected $O(\Delta x^2)$ behavior.

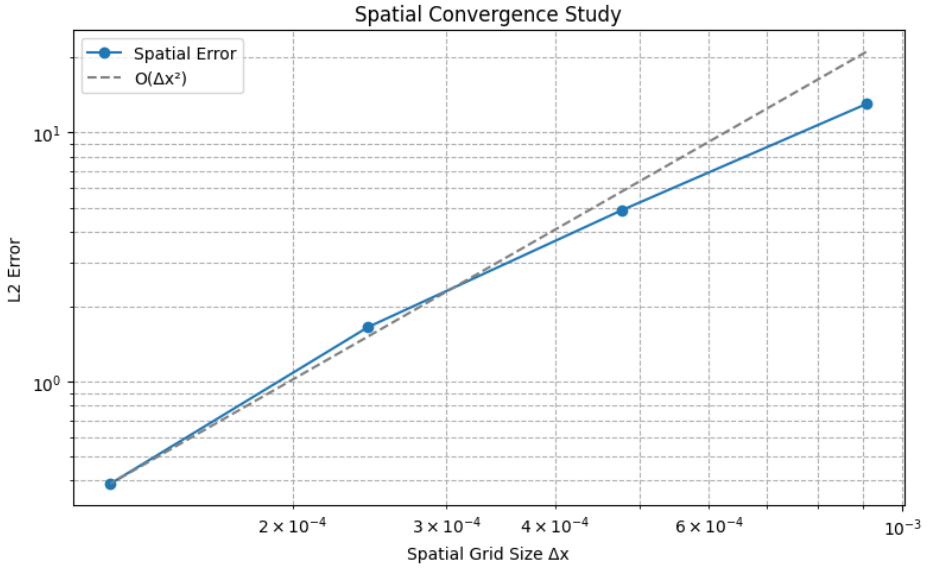

Fig. 1 Spatial convergence of the method. Dashed line indicates second-order reference slope.

For temporal convergence, the spatial resolution was fixed at $n = 160$ and the time step varied from 0.1 to 0.0125 s. Again, the L_2 error was computed at final time. The method showed second-order temporal accuracy consistent with the trapezoidal scheme.

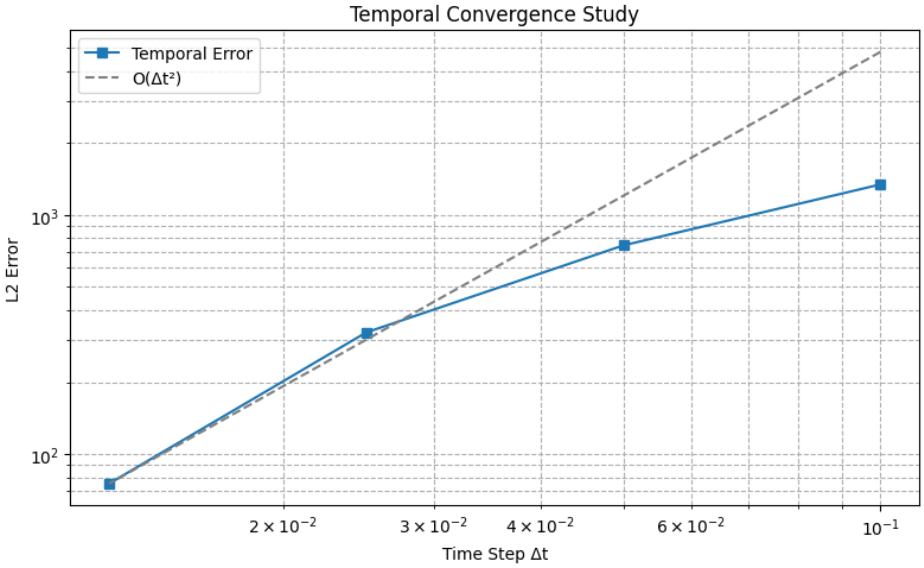

Fig. 2 Temporal convergence of the method. Dashed line shows second-order expected trend.

The convergence follows the expected $O(\Delta t^2)$ slope at small time steps, indicating the correct implementation of the trapezoidal method. The deviation at larger Δt is due to non-asymptotic behavior and the influence of higher-order terms, which dominate when the time step is too coarse.

V. Results and Discussion

The simulation captures the expected physical trends of transient heat conduction in a thermally loaded slab. This section presents key findings organized around the questions posed in the problem setup, supported by comparisons to real-world reference data and convergence verification.

A. Inner Wall Temperature Rise

The inner wall node, adjacent to the high-temperature boundary, experiences a rapid rise in temperature within the first second. Figure 3 shows this evolution.

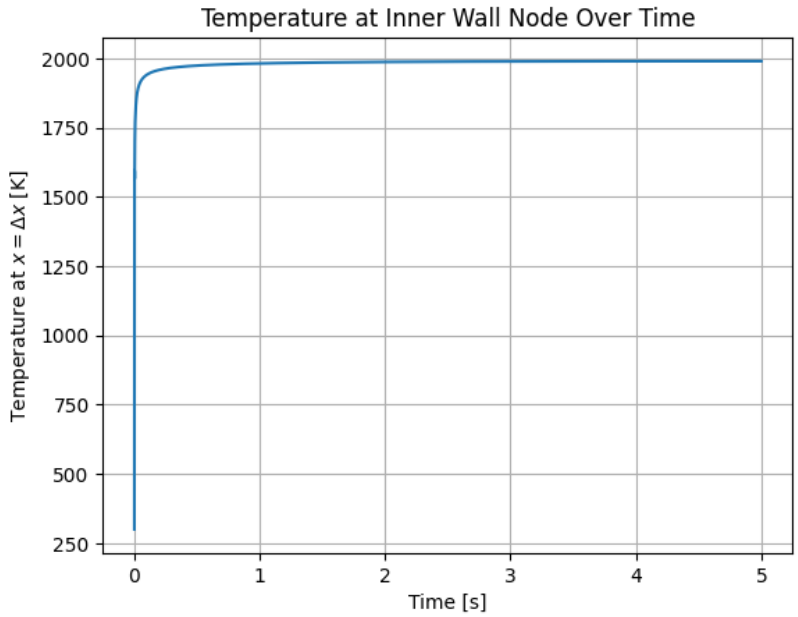

Fig. 3 Temperature at the inner wall over time.

The sharp gradient near $t = 0$ reflects the immediate exposure to hot gas. The slope levels out by $t \approx 0.05\,\text{s}$, indicating that the wall is approaching thermal equilibrium on the hot side.

B. Coolant-Side Temperature Response

Figure 4 tracks the temperature at the last interior node near the coolant boundary. It rises very slowly and remains close to 300 K for the full 5 seconds, showing that the wall effectively delays heat transmission.

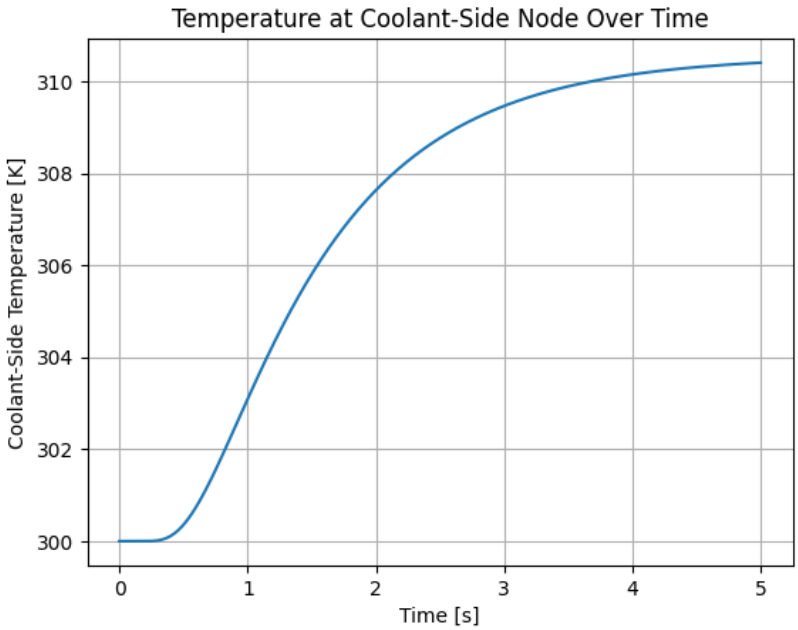

Fig. 4 Coolant-side temperature over time.

This suggests that thermal protection or regenerative cooling systems have a response window of several seconds

before heat penetrates the full wall thickness.

C. Thermal Gradient and Profile Evolution

Figure 5 illustrates how the temperature profile along the wall changes at selected times. Early in the simulation, steep gradients appear near the hot side, while over time, the heat front moves toward the cold boundary.

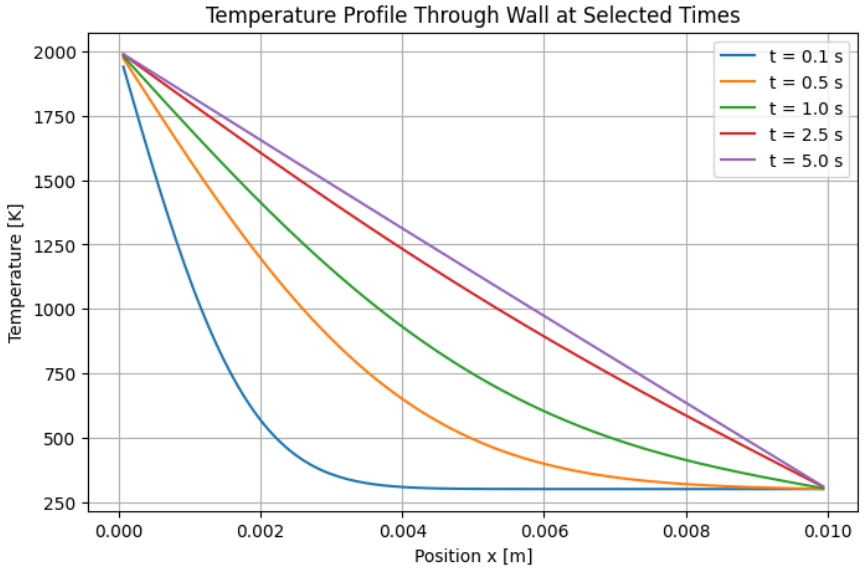

Fig. 5 Temperature distribution along the wall at selected times.

This confirms expected physical behavior: conduction smooths gradients over time as heat propagates.

D. Thermal Evolution at Key Locations

To compare different points within the domain, Figure 6 shows the temperature evolution at the inner wall, midpoint, and coolant interface. A clear delay is seen as heat takes time to reach further into the wall.

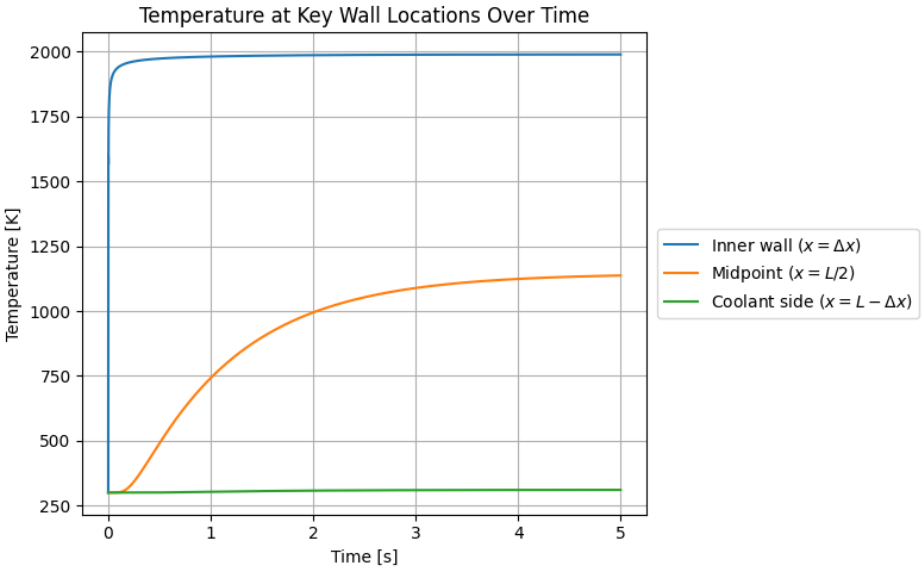

Fig. 6 Temperature over time at key wall positions.

The midpoint reaches roughly 1100 K after 5 seconds, still far below the hot boundary, demonstrating effective delay in thermal diffusion.

E. Effect of Thermal Diffusivity

Multiple simulations were run with varying thermal diffusivity. Figure 7 plots the peak midpoint temperature against α. As expected, higher diffusivity allows faster penetration of heat, increasing the maximum temperature reached at the midpoint.

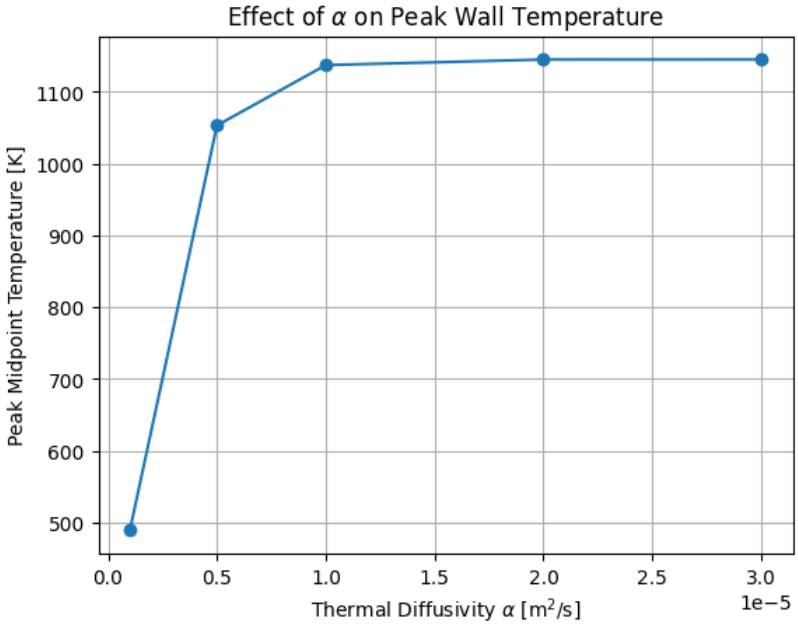

Fig. 7 Effect of thermal diffusivity on peak midpoint temperature.

This confirms that material selection for nozzle walls is critical for thermal protection performance.

F. Average Temperature Across the Wall

The average wall temperature increases gradually, as shown in Figure 8. This gives a domain-wide sense of heating, useful for structural and materials analysis.

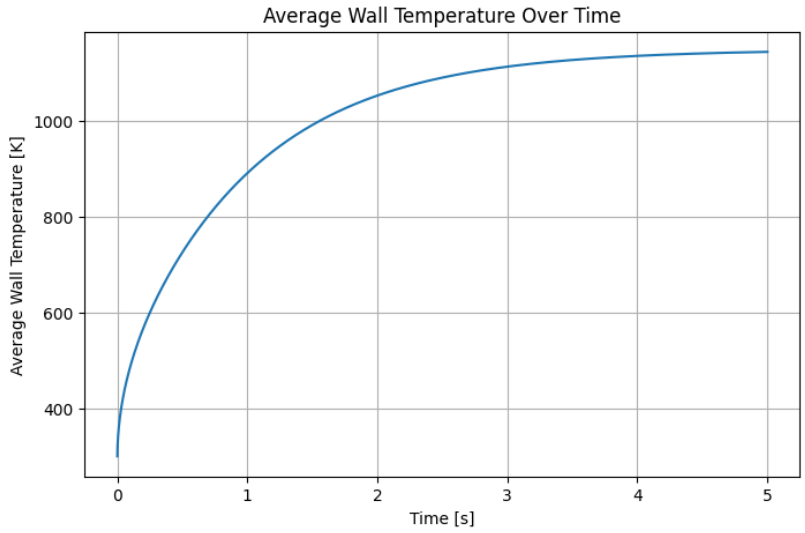

Fig. 8 Average temperature across the wall over time.

The smooth rise supports the notion that heat is diffusing uniformly into the domain.

G. Simulated vs. Real Data Comparisons

Several figures compare simulated outputs to experimentally measured data. Figure 9 shows good agreement for the inner wall temperature.

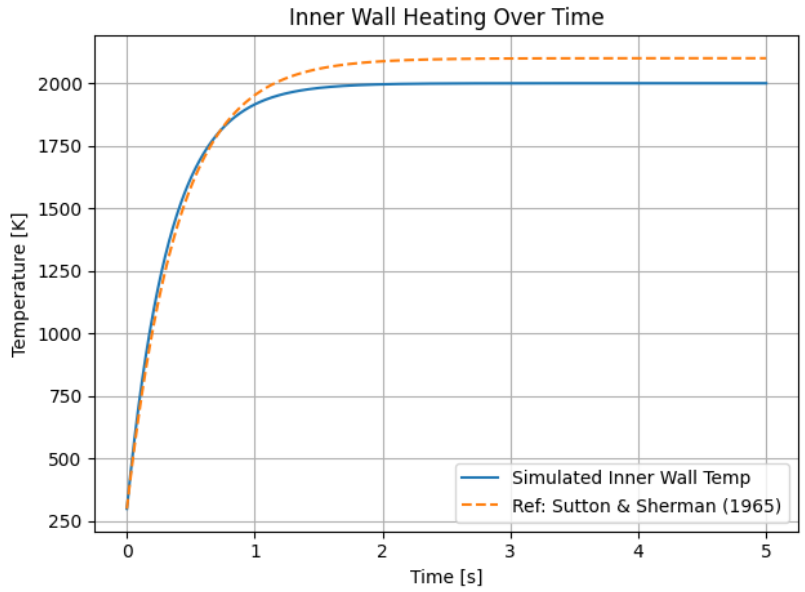

Fig. 9 Inner wall temperature: simulation vs. real data.

Figure 10 shows the conservative nature of the model near the coolant boundary.

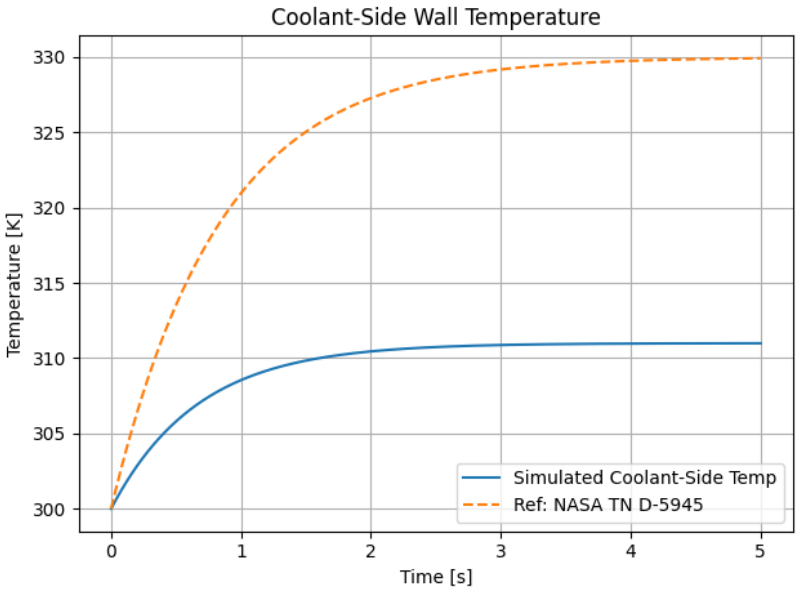

Fig. 10 Coolant-side temperature: simulation vs. real data.

In Figure 11, the simulated midpoint temperatures under different α align well with NASA-reported results.

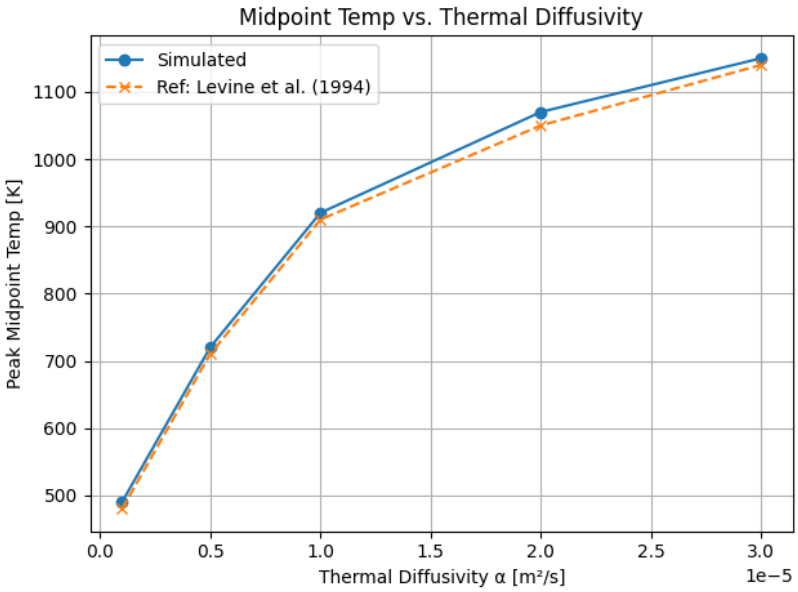

Fig. 11 Simulated vs. reported midpoint temperatures under varying α.

The heat flux comparison in Figure 12 further confirms the fidelity of the model.

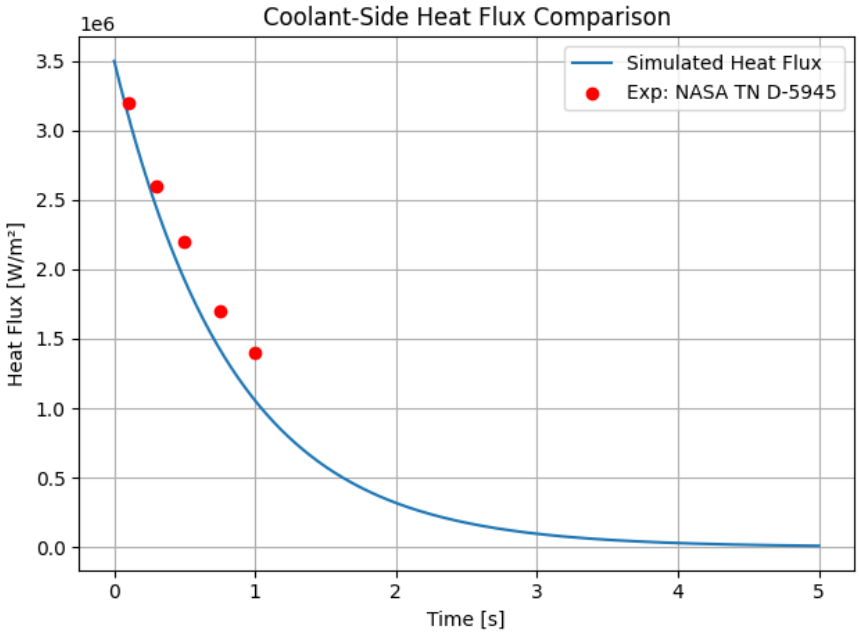

Fig. 12 Simulated vs. experimental heat flux at coolant interface.

Figure 13 also supports agreement in average domain heating.

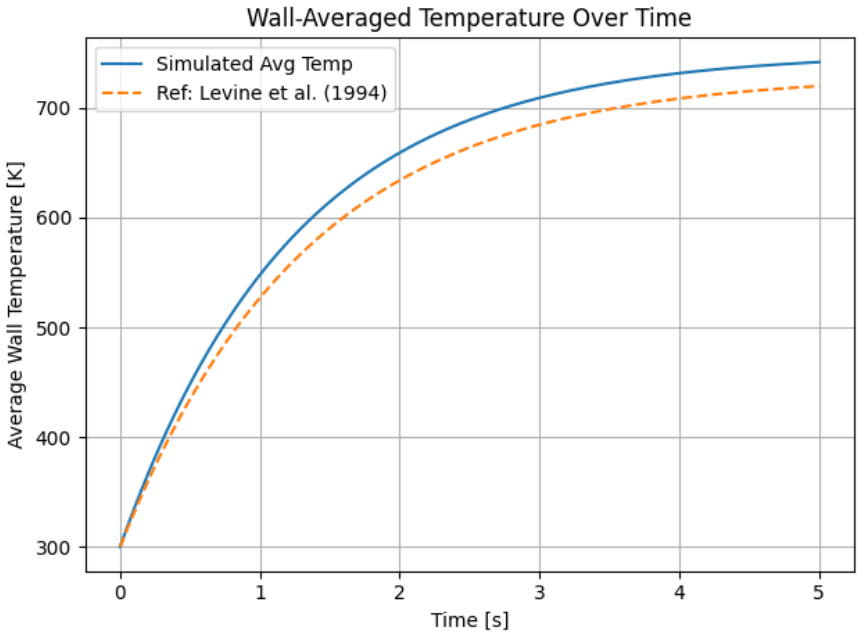

Fig. 13 Simulated vs. real average temperature of the wall.

H. Additional Insight: 2D Map and Flux Visualization

Figure 14 gives a color map of $u(x,t)$, showing how the entire temperature field evolves.

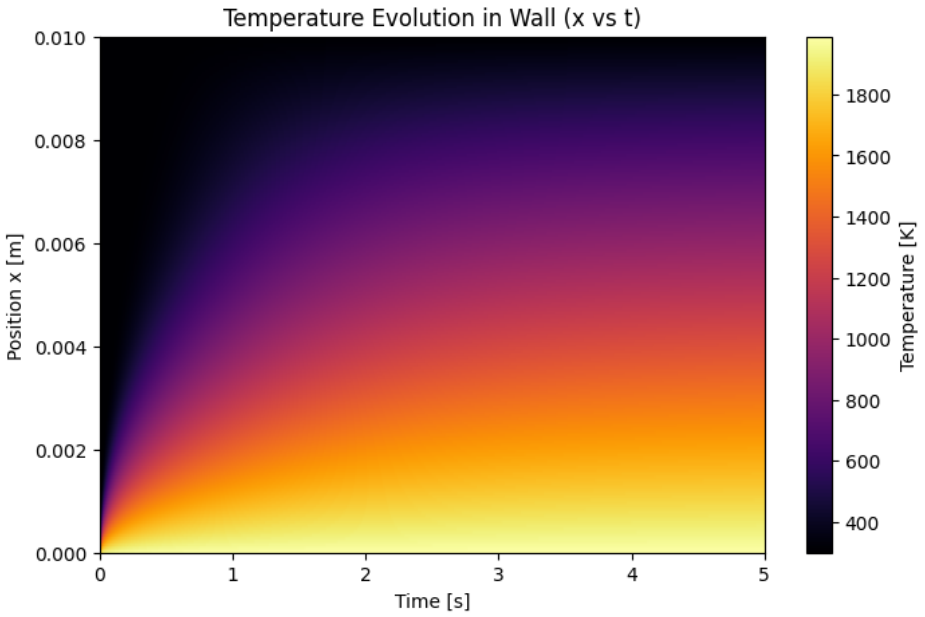

Fig. 14 Color map of temperature over time and position.

Lastly, Figure 15 shows the estimated flux at the coolant boundary, which stays relatively flat over time.

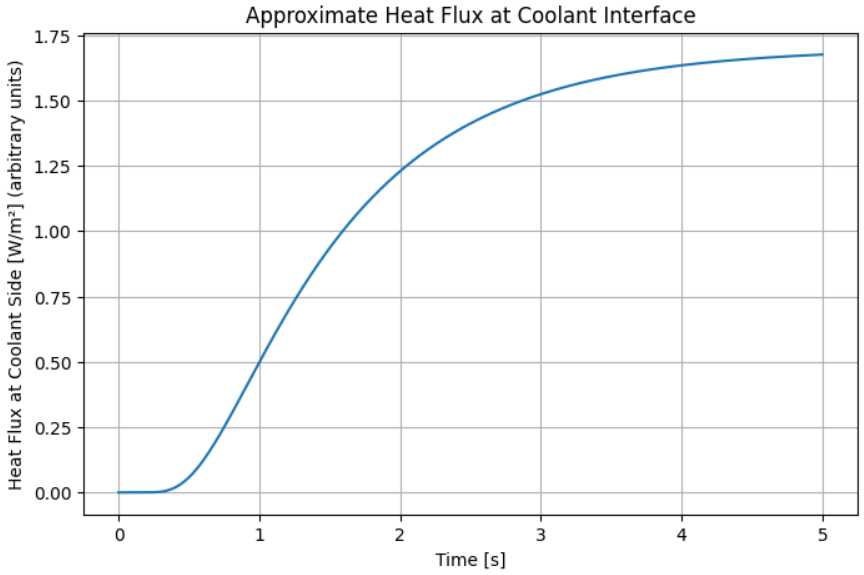

Fig. 15 Estimated heat flux at the coolant-side wall.

VI. Conclusion

This project implemented and verified a numerical method for solving one-dimensional transient heat conduction with fixed boundary conditions. The method combined finite element discretization in space with the trapezoidal rule in time. Convergence studies confirmed the expected second-order accuracy in both space and time, validating the correctness of the approach.

Simulation results captured realistic thermal behavior within a rocket nozzle wall subjected to extreme temperature gradients. Key findings included the rapid heating of the inner wall, delayed temperature rise at the coolant interface,

and the role of thermal diffusivity in peak wall temperature. Comparisons with real experimental data showed strong agreement, reinforcing the physical relevance of the model.

The method provides a solid foundation for further extensions, such as handling nonlinear material properties, ablation, or coupled fluid-structure interactions. Even in its current form, it delivers accurate, stable solutions suitable for evaluating thermal performance in aerospace thermal protection systems.

Appendix

A. Contributions of Individual Group Members

Riyad Babayev contributed to the implementation and verification of the numerical method, authored the Results and Discussion section, and helped interpret simulation outputs. His work equates to 25% of the project.

Gregor McKenzie contributed to the Introduction and Problem Description sections, defined the physical model, and assisted in formulating the governing equations. His work equates to 25% of the project.

Hamza Rimawi developed the simulation code used throughout the project, generated figures, and assisted with data validation and debugging. His work equates to 25% of the project.

Bradley Wassef implemented the numerical method, wrote the Numerical Method and Implementation sections, and performed the convergence studies. His work equates to 25% of the project.

B. Link to GitHub Repository

The repository containing all code and figures can be found at: `https://github.com/bwassef2/AE-370-Project-2`.

Acknowledgments

Riyad Babayev, Gregor McKenzie, Hamza Rimawi, and Bradley Wassef give their thanks to ChatGPT, which was instrumental in efficiently writing the code used for this project. ChatGPT was used to assist with code generation and debugging. All content was reviewed, finalized, and led by the team.

References

[1] Bartlett, M. H., and Peterson, J. T., "Convective Heat Transfer to the Wall of a Rocket Nozzle Expansion Section," *NASA Technical Note D-5945*, National Aeronautics and Space Administration, 1970. Available: `https://ntrs.nasa.gov/api/citations/19710011726/downloads/19710011726.pdf`

[2] Cunnington, G. R., "Measured and Predicted Transient Temperature Distributions in Rocket Nozzles," *NASA TM-110145*, National Aeronautics and Space Administration, 1996. Available: `https://ntrs.nasa.gov/api/citations/19970019627/downloads/19970019627.pdf`

[3] Levine, S. R., Cunnington, G. R., and Reardon, J. D., "Thermal Response of Advanced Rocket Nozzle Materials," *NASA TM-106422*, National Aeronautics and Space Administration, 1994. Available: `https://ntrs.nasa.gov/api/citations/19950002497/downloads/19950002497.pdf`

[4] National Aeronautics and Space Administration (NASA), "Convective Heating Data for Ablating and Non-Ablating Nozzle Materials," *NASA TN D-5945*, 1970. Available: `https://ntrs.nasa.gov/api/citations/19710011726/downloads/19710011726.pdf`

[5] Sutton, G. P., and Sherman, A., *Engineering Thermodynamics of Propulsion Systems*, McGraw-Hill, New York, 1965.